SCIENCE CHINA
Physics, Mechanics & Astronomy

• Article •

February 2015 Vol. 58 No. 2: 024602
doi: 10.1007/s11433-014-5595-x

Residual stress of physical vapor-deposited polycrystalline multilayers

ZHANG Song[1], ZHANG Hui[2] & ZHENG LiLi[1*]

[1] *School of Aerospace, Tsinghua University, Beijing 100084, China;*
[2] *Department of Engineering Physics, Tsinghua University, Beijing 100084, China*

Received March 14, 2014; accepted August 20, 2014; published online October 14, 2014

An extended one-dimensional stress model for the deposition of multilayer films is built based on the existing stress model by considering the influence of deposition conditions. Both thermal stress and intrinsic stress are considered to constitute the final residual stress in the model. The deposition process conditions such as deposition temperature, oxygen pressure, and film growth rate are correlated to the full stress model to analyze the final residual stress distribution, and thus the deformation of the deposited multilayer system under different process conditions. Also, the model is numerically realized with in-house built code. A deposition of Ag-Cu multilayer system is simulated with the as-built extended stress model, and the final residual stresses under different deposition conditions are discussed with part of the results compared with experiment from other literature.

growth models, stresses, physical vapor deposition processes, polycrystalline deposition, metals

PACS number(s): 68.55.Ac, 68.55.Jk, 68.65.Ac, 83.85.St, 62.20.Fe

Citation: Zhang S, Zhang H, Zheng L L. Residual stress of physical vapor-deposited polycrystalline multilayers. Sci China-Phys Mech Astron, 2015, 58: 024602, doi: 10.1007/s11433-014-5595-x

1 Introduction

EB-PVD has been demonstrated to be of great use in film deposition. Residual stress always occurs in a physical vapor-deposited multilayer system, causing either delamination or crack of the films. Hence, it is of great importance for the use of coated products to control the residual stress level in deposited multilayer systems. It is believed that the residual stress is constituted by thermal stress and intrinsic stress, and both are related to thermal transport and growth process. The thermal stress is generated because of the mismatch between thermal expansion coefficients of substrate and film material when subjected to the same cooling process. The intrinsic stress is the stress generated during the film growth process of films. Much work has been reported with regard to the stress generation during the deposition process of a multilayer system.

Physical vapor deposition involves the atoms' deposition and diffusion onto the substrate and the films grow into columnar grains in a Volmer Weber mode [1–4] for most cases of polycrystalline film deposition. Floro and his coworkers [1,2] investigated the physical origin of Volmer Weber films that are mostly polycrystalline films (including amorphous films like a-Ge films on SiO_2 films). They found that the stress always appears to undergo a compressive tensile compressive process. During the deposition of films, the compressive stress generated initially by the surface stress of the formed island is quickly changed to tensile stress because of the formation of a continuous film by the island coalescence and then followed by the compressive stress [3,4]. Many theoretical and experimental studies [4–16] have been conducted to study the stress generation including thermal stress and intrinsic stress during the deposition

*Corresponding author (email: zhenglili@tsinghua.edu.cn)

process of a polycrystalline multilayer system. However, each of these works just expressed part of the stress generation during the deposition process. Combining all these parts, Song and his coworkers [17] built a comprehensive model to describe the generation and combination of thermal and intrinsic stress during the deposition process. However, the stress generation cannot be connected with the deposition process conditions in the comprehensive model. Different process conditions may influence the deposition process through the nucleation process, surface tension during the growth process, diffusion of atoms, and energy of the upcoming atoms.

The aim of this paper is to build a relationship between the deposition conditions and the residual stress of a multilayer system by linking the deposition conditions with parameters needed in the stress model such as nucleation rate, surface tension, grain boundary energy, and chemical potential. In this paper, an extended model is developed to describe the stress generation during the deposition of polycrystalline multilayers under different process conditions such as temperature, pressure, and film thickness.

2 Physical and mathematical models for stress generation

The thermal residual stress for a multilayer system is generated when a temperature change occurs because the thermal expansion of the substrate and films do not match each other. Song and his coworkers [17] built a thermal stress model for multilayer systems based on the conservation of force and moment. They also added the intrinsic stress in the thermal stress model.

The thermal residual stress in Figure 1 can be obtained as:

$$\begin{aligned}\sigma_{\mathrm{s}} &= E_{\mathrm{s}}\left(c+\frac{z-t_{\mathrm{b}}}{r}-\alpha_{\mathrm{s}}\Delta T_z+\varepsilon_{\mathrm{s},z}\right),\\ \sigma_i &= E_i\left(c+\frac{z-t_{\mathrm{b}}}{r}-\alpha_i\Delta T_z+\varepsilon_{i,z}\right),\end{aligned} \tag{1}$$

where σ_{s} and σ_i are the stresses in substrate and layer i, c is the uniform strain component in Figure 1(c), α_i and α_{s} are the thermal expansion coefficients of the substrate and film material, T_z is the temperature distribution along the Z direction, and $\varepsilon_{\mathrm{s},z}$ and $\varepsilon_{\mathrm{i},z}$ are the intrinsic stresses distribution along the Z direction. The intrinsic stresses are obtained in the model by considering the atoms' flowing and nucleation during the film growth process. Combining the intrinsic stresses into the quasi-static thermal stress model by considering the conservation of force and moment, the thermal stress and intrinsic stress are coupled and the final residual stress can be obtained.

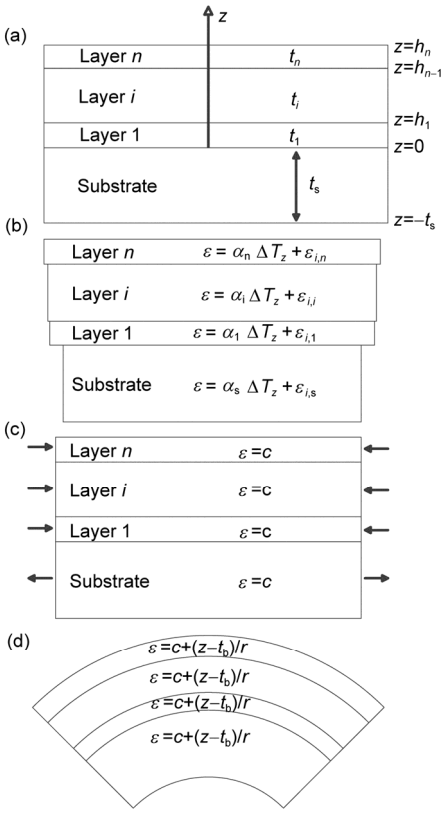

Figure 1 Schematic of the deformation and stress evolution of a multilayer system under a temperature decrease: (a) multilayer system and coordinate system; (b) unconstrained strain because of temperature decrease with intrinsic strain included; (c) strain constrained by displacement compatibility, and (d) bending of the system.

The uniform strain component c in Figure 1(c) can be expressed as:

$$c=\frac{E_{\mathrm{s}}\int_{-t_{\mathrm{s}}}^{0}\left(\alpha_{\mathrm{s}}\Delta T_z-\varepsilon_{\mathrm{s},z}\right)\mathrm{d}z+\sum_{i=1}^{n}E_i\int_{h_{i-1}}^{h_i}\left(\alpha_i\Delta T_z-\varepsilon_{i,z}\right)\mathrm{d}z}{E_{\mathrm{s}}t_{\mathrm{s}}+\sum_{i=1}^{n}E_it_i}, \tag{2}$$

t_{b} is the location of bending axis that can be expressed as:

$$t_{\mathrm{b}}=\frac{-E_{\mathrm{s}}t_{\mathrm{s}}^2+\sum_{i=1}^{n}E_it_i\left(2h_{i-1}+t_i\right)}{2\left(E_{\mathrm{s}}t_{\mathrm{s}}+\sum_{i=1}^{n}E_it_i\right)}, \tag{3}$$

and r is the radius of curvature of the bending system that can be denoted as:

$$\frac{1}{r}=\frac{3\left[E_{\mathrm{s}}ct_{\mathrm{s}}^2-\sum_{i=1}^{n}E_ict_i\left(2h_{i-1}+t_i\right)\right]-6E_{\mathrm{s}}\int_{-t_{\mathrm{s}}}^{0}\left(-\alpha_{\mathrm{s}}\Delta T_z+\varepsilon_{\mathrm{s},z}\right)z\mathrm{d}z-6\sum_{i=1}^{n}E_i\int_{h_{i-1}}^{h_i}\left(-\alpha_i\Delta T_z+\varepsilon_{i,z}\right)z\mathrm{d}z}{E_{\mathrm{s}}t_{\mathrm{s}}^2\left(2t_{\mathrm{s}}+3t_{\mathrm{b}}\right)+\sum_{i=1}^{n}E_it_i\left[6h_{i-1}^2+6h_{i-1}t_i+2t_i^2-3t_{\mathrm{b}}\left(2h_{i-1}+t_i\right)\right]}. \tag{4}$$

In the model of thermal stress, the residual strain of the substrate after annealing is set as the intrinsic strain term $\varepsilon_{s,z}$.

The intrinsic stress is stress generated in the process of film growth and will undergo compressive tensile compressive states during deposition of a single-layer polycrystalline film. In the model of Song and his coworkers [17], the intrinsic stress level is mainly related to the nucleation, island growth, and coalescence and incorporation of atoms into the grain boundary. However, links between deposition conditions and the related process are still needed to build the links between final residual stress and deposition conditions.

In the early stage of film growth, evaporated atoms are absorbed onto the baseplate and nucleate at a nucleation rate of N_s. The nucleation rate can be obtained using the kinetic model for nucleation [18] as:

$$N_s = An_0 \left| \frac{\dot{R}}{n_0 v} \right|^{p'} \exp\left(\frac{E'}{RT} \right), \tag{5}$$

where A is a calculable dimensionless constant dependent on the substrate coverage, n_0 is the density of adsorption sites, and v is the vibrational frequency of adatoms on the surface. The parameters p' and E' are discussed in Appendix A.

The nucleus absorbs the evaporated atoms and grows into a spherical island. The shape of the island is decided by the equilibrium of the three kinds of surface tension that can be expressed as:

$$\gamma_{sv} = \gamma_{ls} + \gamma_{vl} \cos\theta, \tag{6}$$

where θ is the wetting angle of the island, γ_{vl} is the surface tension between the island surface and vapor, γ_{ls} is the surface tension between the island and baseplate, and γ_{sv} is the surface tension between the baseplate and vapor. The surface tension of metal can be obtained as follows:

$$\gamma = \frac{nZ_\gamma}{N_0 Z_0} \Delta H_v, \tag{7}$$

where n is the number of atoms per area, Z_0 is the body coordination number, Z_γ is the interface coordination number that is defined as $(Z_0 - Z_s)/2$, that Z_s is the surface coordination number. N_0 is the Avogadro's number and ΔH_v is the heat of vaporization. The contact interface energy can be obtained by an average of the surface energy of each separate metal. The derivation of the surface energy of metal is shown in Appendix B.

Following Hoffman [5] and Nix and Clemens [6] and considering the island snapping together and boundary formation as a crack-closure process, the planar strain along the Z direction can be obtained as:

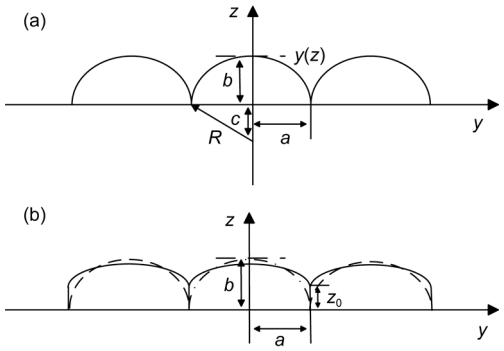

Figure 2 Schematic of the island coalescence: (a) shape of the island before coalescence and (b) shape of the islands after coalescence.

$$\varepsilon(z) = 1 - \frac{1}{\sin\theta}\left[1 - \left(\frac{z+c}{R} \right)^2 \right]^{1/2}, \tag{8}$$

where $R = a/\sin\theta$, $c = a\cot\theta$, and $b = a/\sin\theta - a\cot\theta$ as shown in Figure 2(a) and a is the average radius of the islands $1/\sqrt{3N_s}$.

The contact height z_0 in the snap process is obtained by solving for the average stress [6]:

$$\langle\sigma\rangle = \frac{E}{1-v^2}\frac{1}{z_0}\int_0^{z_0} \varepsilon(z)\mathrm{d}z = \left[\left(\frac{1+v}{1-v} \right) E \frac{(2\gamma_{vl} - \gamma_{gb})}{a} \right]^{1/2}, \tag{9}$$

where γ_{vl} is the surface free energy of the islands and γ_{gb} is the grain boundary energy. The right side term in eq. (9) is the average stress generated during the coalescence process that is obtained by treating the boundary formation as a crack-closure process.

The grain boundary energy as a function of misorientation is assumed to follow the Read-Shockley equation [19]:

$$\frac{\gamma_{gb}}{(\gamma_{gb})_m} = \frac{\theta}{\theta_m}\left(1 - \ln\frac{\theta}{\theta_m} \right), \tag{10}$$

where θ is the misorientation across the grain boundary and θ_m is the critical misorientation and $(\gamma_{gb})_m$ is the grain boundary energy when the misorientation is larger than θ_m. In this work, θ_m is set as 15° and $(\gamma_{gb})_m$ used the value of 0.625 J/m [20].

The contact height can be calculated numerically and expressed as:

$$z_0 = f(a, b, c, v, E, \gamma_{vl}, \gamma_{gb}). \tag{11}$$

When the coalescence process is finished, grain boundaries are formed. During post coalescence growth, the upcoming atoms are incorporated into the grain boundary (see Figure 3) driven by the chemical potential difference between atoms

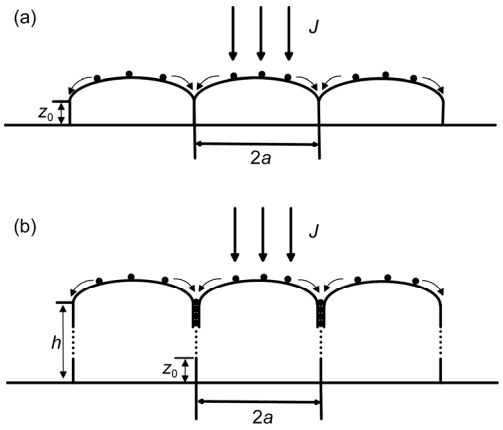

Figure 3 Schematic of adatoms flowing into the grain boundary. (a) Grain boundary formed after island coalescene; (b) adatoms flowing into the grain boundary during film growth.

on the surface and in the boundary.

During the deposition process, atoms on the surface are in nonequilibrium conditions that have a higher chemical potential than when they are in equilibrium conditions. We assume that atoms on the surface are in equilibrium with the gaseous atoms, and thus the chemical potential increment because of the impinging of atoms can be expressed as:

$$\delta\mu_{\text{sur}} = kT\ln\left(\frac{p}{p_0}\right), \tag{12}$$

where p_0 is the saturated vapor pressure under the given temperature. Thus the chemical difference between the surface and the grain boundary is

$$\Delta\mu = \Delta\mu^0 + kT\ln\left(\frac{p}{p_0}\right) + \sigma\Omega, \tag{13}$$

where we define $\Delta\mu^0 = \mu^0_{\text{sur}} - \mu^0_{\text{gb}}$ as the chemical potential difference between the surface and the grain boundary in equilibrium, σ is the normal stress acting across the grain boundary.

The stress changes with time at a rate of [4]:

$$\frac{\partial\sigma}{\partial t} = -\left(\frac{\sigma_0 a_0}{h}\right)2C\Gamma\left(\frac{\Delta\mu^0 + \delta\mu_{\text{sur}} + \sigma\Omega}{kT}\right) + (\sigma_i - \sigma)\frac{R_{\text{growth}}}{h}. \tag{14}$$

In the multilayer system, experimental results [21] show that there is a nucleation process at the beginning of the deposition of each new layer. The former films and the substrate can be regarded as a new substrate and the new film is deposited at the new substrate. Thus the intrinsic stress of the new layer is generated in the same way as in the first layer except that the nucleation process occurs at a surface with angular crystal surface.

3 Computational method

The stress generation in the deposition of multilayer system is studied numerically using the extended model. Different conditions of temperature, film thickness, pressure in deposition chamber, and film growth rate are considered in the model. Also, the intrinsic strain and thermal strain are combined to predict the final film stress in the multilayer system. Figure 4 shows the flow chart of the computational model. Because the temperature may change during the deposition of each layer, the thermal and growth processes are simulated in every cycle of the film deposition. The thermal stress analysis is conducted using the thermal stress model with the intrinsic stress generated in the growth process as

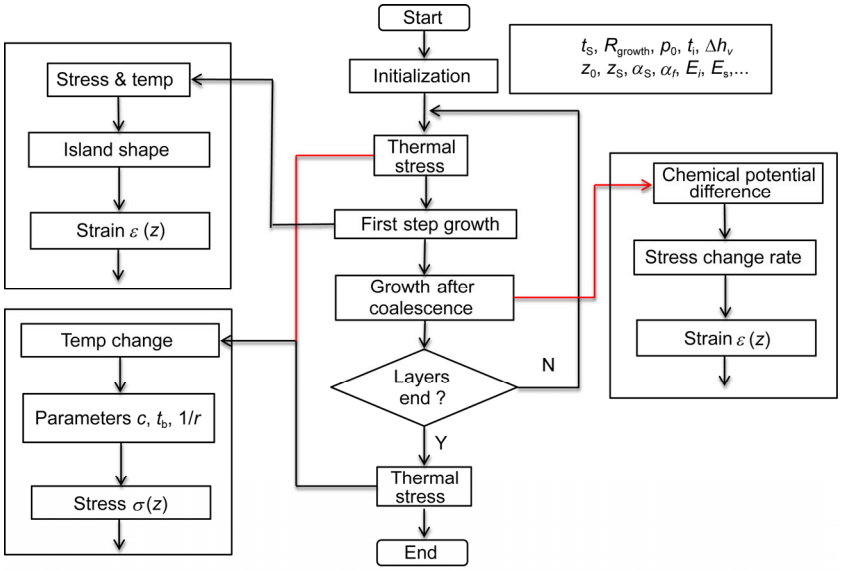

Figure 4 (Color online) The computational process of the stress analysis model.

initial conditions. At the end of the deposition process, a cooling process, which is mainly responsible for thermal stress generation is initiated. The growth process can be divided into two sub-processes: island coalescence and growth after coalescence. In the island coalescence process, the island shape is decided by the process-influenced parameters. The planar strain along the Z direction is calculated based on the island shape. In this process, the island shape can be influenced by the surface residual stress of the film system which can be obtained from the thermal stress analysis in the present cycle in Figure 4. The surface residual stress can influence the island shape by influencing the surface energy. The strain after island coalescence is calculated using the model in eq. (14). During the calculation of strain generation after coalescence, the final residual stress generated during the coalescence process is set as initial conditions for the growth process after coalescence.

4 Results and discussion

The thermal stress model is validated using the mathematical solution for the thermal stress in a single layer film system which is widely accepted. And the intrinsic model is validated using the experimental work of Shull et al. [21]. As the model is validated, the influence of the process conditions such as deposition temperature, pressure in the deposition chamber, film growth rate, and film thickness on the final residual stress is discussed. The thickness ratio is used to represent the film thickness. When the layer thicknesses are changed, the thickness ratio is expressed as:

$$\eta = \frac{1+\phi}{1-\phi} \times 100\%, \tag{15}$$

where ϕ is the percentage of Cu layer thickness variation and $-\phi$ is the percentage of Ag layer thickness variation (using the convention that increment is positive).

4.1 Stress model validation

To validate the thermal stress model, the thermal stress in a one-layer film system is simulated using the multilayer thermal stress model. A case of 19.7-nm Cu layer deposited on a 108-μm Si (100) substrate at 40°C, and then cooled to a room temperature of 20°C is studied and Table 1 shows the thermal and mechanical properties used in the simulation. The simulation result is compared with mathematical solution [24]:

$$\sigma_f = \frac{E_{\mathrm{Cu}}\left(\alpha_{\mathrm{Si}} - \alpha_{\mathrm{Cu}}\right)\Delta T}{1+4\left(E_{\mathrm{Cu}}/E_{\mathrm{Si}}\right)\left(h/H\right)}. \tag{16}$$

The simulation result of the average thermal stress in the film using the mathematical model is 23.2774 MPa, whereas the simulation model obtains a result of 23.2768 MPa. Comparison shows that the thermal stress model has little difference with the mathematical solution.

Table 2 shows the thermal dynamic properties of Cu and Ag that are used in the simulation. The data for Ag used in the simulation of deposition process can be obtained from other literature [4,18] as listed in Tables 3 and 4. The deposition of 535 nm Cu on the Si (100) substrate is simulated and compared with the experiment results [21] to get the data needed for Cu in the model. Only the first layer of a deposition of multilayer is chosen and the results show that the simulation result and the experimental result expressed as F/w (total force per unit width) meet each other very well (see Figure 5). Thus, the data needed for Cu is obtained and listed in Tables 3 and 4. The deposition rate used in the

Table 1 Thermal and mechanical properties used in the simulation [22,23]

Material	Thermal conductivities (W m^{-1} K^{-1})	Thermal expansion coefficient (10^{-6} K^{-1})	Young's modulus (GPa)	Poisson's ratio
Si	148	7.6	113	0.28
Cu	401	16.7	128	0.35
Ag	429	19.0	71	0.38
Al	237	–	–	–

Table 2 Thermal dynamic properties used in the simulation

Material	Body coordinate number	Surface coordinate number	Lattice size (pm)	Heat of vaporization (kJ mol^{-1})
Cu	12	4	361.49	306.89
Ag	12	4	408.53	284.6

Table 3 Data used in nucleation dynamics [18]

Material	E_{des} (eV)	E_{s} (eV)	v (10^{12} s^{-1})	n_0 (atoms m^{-2})	Atom number per volume (10^{30})	Volume of atom (10^{-29} m^3)
Cu	0.7	0.3	1.65	1.0×10^{19}	4.2742	2.3396
Ag	0.5	0.2	0.1	1.0×10^{20}	6.2006	1.61275

Table 4 Data used in the simulation of process after coalescence [4]

Material	$2C_s\Gamma(s^{-1})$	$\Delta\mu_0$ (10^{-22} J mol^{-1})	Ω (10^{-29} m^3)
Cu	3.3	50.2	1.7
Ag	3.3	4.02	1.7

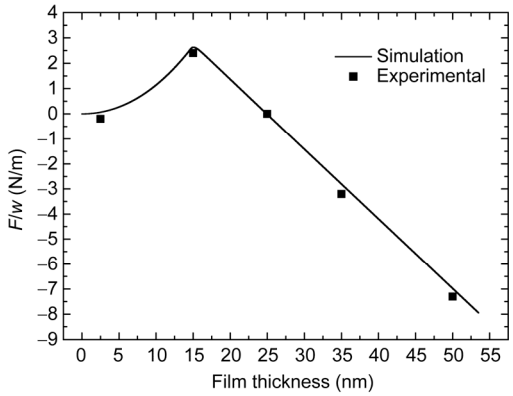

Figure 5 Compare of simulation and experimental results for Cu on Si substrate [21].

experiment was 0.01 nm/s and the pressure was 1.20×10^{-6} Pa for Cu and 6.67×10^{-7} Pa for Ag.

To validate the whole intrinsic stress model, another set of experimental work of Shull et al. [21] is simulated with the data obtained in the simulation of deposition of single Cu layer. In this work, 10 layers of Cu and Ag are deposited on a 108-μm Si (100) substrate alternately at a low temperature. The layer thicknesses are as: Cu 19.7 nm / Ag 15 nm / Cu 12.4 nm / Ag 15 nm /Cu 10.8 nm / Ag 15 nm / Cu 10.8 nm / Ag 15 nm / Cu 10.8 nm / Ag 15 nm.

Figure 6 shows the comparison of the experimental and simulation results. The average stress of the multilayer system is 42 MPa in the experiment and the simulation obtained a 43.6 MPa film average stress. During the early stage of deposition, the difference between experiment and simulation is a little greater, which is possibly caused by the difference between the process conditions of the experiment and simulation.

4.2 Discussion of results

To investigate the influence of process conditions on the final residual film stress, deposition of 10 layers under different deposition temperature, pressure, film growth rate, and film thickness are simulated. The simulation results are compared with only one variable and the baseline case is the case in Figure 6.

Figure 7 shows the simulation result when the thermal stress is considered and the result is also compared with the intrinsic stress. The result shows that there is a tensile thermal stress in the film and thus increases the film average stress from 43.6 MPa to 58.0 MPa. The thermal stress accounts for 24.8% of the final residual stress of the film and

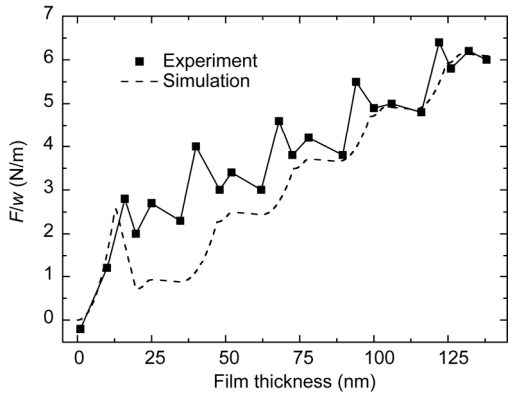

Figure 6 Comparison of experimental and simulation results for the baseline case [21].

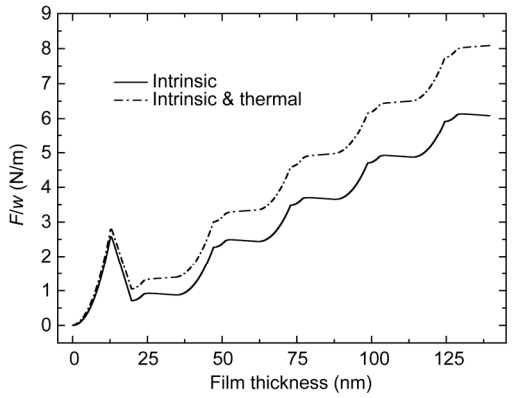

Figure 7 *F*/*w* versus total film thickness for cases when only intrinsic stress or both intrinsic stress and thermal stress are considered.

it is important to consider both intrinsic and thermal stress because both of them are influenced by the deposition conditions.

Deposition temperature can influence both the thermal stress and the film growth process and thus the intrinsic stress. Figure 8 shows *F*/*w* evolution with film thickness under different deposition temperatures. It is shown that under the simulated conditions the final residual stress increases with the deposition temperature. When the deposition temperature increased from 30°C to 50°C, the average stress increased from 51.9 MPa to 66.9 MPa. The thermal mismatch stress will increase with the increase in deposition temperature because the thermal expansion mismatch will increase. In Figure 8, there is a shift of the first peak value to the right which indicates that the contact height in the coalescence process increases with the increase of deposition temperature. This is caused by the reason that the nucleation rate will decrease at a higher deposition temperature, and this will lead to a higher average grain size for the nucleus when they snap together. From the earlier discussion, it can be seen that a higher average grain size will lead to a higher contact height and a higher tensile stress during the coalescence process.

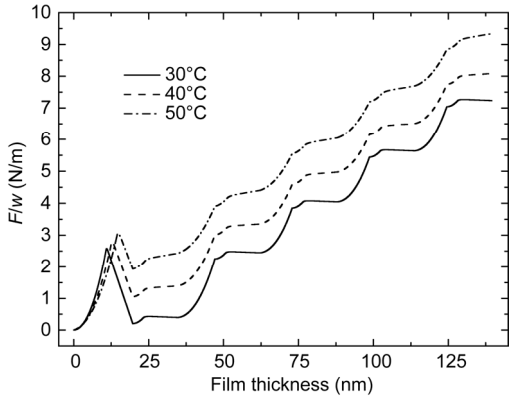

Figure 8 *F*/*w* versus total film thickness under different deposition temperatures when both intrinsic stress and thermal stress are considered.

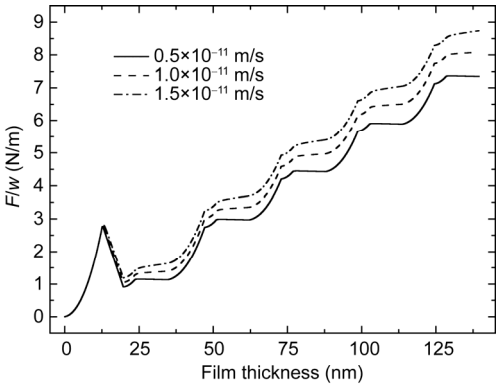

Figure 10 *F*/*w* versus total film thickness under different deposition rates when both intrinsic stress and thermal stress are considered.

The pressure in the chamber can both influence the coalescence process and the atoms incorporation process. Hence, the deposition pressure will mainly influence the intrinsic stress. Figure 9 shows the *F*/*w* evolution with film thickness under different pressures. The final residual stress decreases with the increase of deposition pressure. When the deposition pressure increases, there will be more atoms incorporating into the grain boundary because the chemical potential of atoms on the surface will increase. Also, it is shown that the first peak value shifts left with the increase of the deposition pressure which indicates that the contact height during the coalescence process decreases. This also contributes to the lower average stress for a higher deposition pressure.

The film growth rate will influence the growth process mainly by influencing the atoms incorporation process. Figure 10 shows the *F*/*w* evolution with film thickness under different film growth rate. The result shows that when the film growth rate increased from 0.5×10^{-11} m/s to 1.5×10^{-11} m/s, the average residual stress of the film increased from 52.7 MPa to 62.7 MPa. The film growth rate has little influence on the coalescence process when other process conditions remain the same.

When the thickness ratio is changed, the film thickness of different layers will change. The change of the thickness of each layer will influence both the intrinsic and thermal stresses. Figure 11 shows the *F*/*w* evolution with film thickness and the results show the final average stress increased from 35.3 MPa to 81.0 MPa when the film thickness ratio increased from 0.33 to 1.5. However, for different film thicknesses, it is not always the case. The final residual stress for a small film thickness is lower under a high thickness ratio which is the opposite for the large film thickness case.

5 Conclusion

In this paper, an expanded one-dimensional stress model is built based on the existing model. Both thermal and intrinsic stresses are considered for vapor deposition of multilayer polycrystalline films. Influence of deposition conditions including deposition temperature, pressure, film growth rate, and film thickness are added into this expanded model through the influence of nucleation, surface tension, atom diffusion, and atom chemical potential. It is found that during

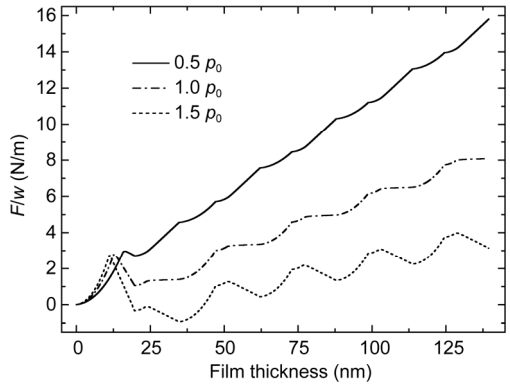

Figure 9 *F*/*w* versus total film thickness under different pressures when both intrinsic stress and thermal stress are considered.

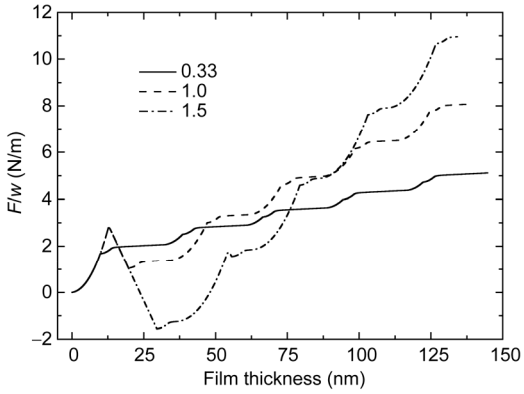

Figure 11 *F*/*w* versus total film thickness under different thickness ratios when both intrinsic stress and thermal stress are considered.

the deposition of polycrystalline multilayer film, intrinsic stress is nearly three times the thermal stress. It is important to consider both the intrinsic and thermal stresses when studying the residual stress of the deposited film. For alternate deposition of Cu and Ag on Si (100) substrate under different deposition conditions, which is studied in this paper, several conclusions can be drawn:

(1) The final residual stress (tensile stress) increases with the increase of deposition temperature.

(2) The final residual stress increases with the decrease of pressure of the evaporated atoms.

(3) Film growth rate has little influence on the final residual stress even a high film growth rate leads to a higher stress level.

(4) Film thickness ratio can strongly influence the final residual stress, and the final residual stress can be changed by adjusting the film thickness ratio.

This work was supported by the National Natural Science Foundation of China (Grant Nos. 51076075, 91224008 and 91024032).

1 Floro J A, Hearne S J, Hunter J A, et al. The dynamic competition between stress generation and relaxation mechanisms during coalescence of Volmer-Weber thin films. J Appl Phys, 2001, 89(9): 4886–4897
2 Floro J A, Chason E, Cammarata R C, et al. Physical origins of intrinsic stresses in Volmer-Weber thin films. MRS Bull, 2002, 27(1): 19–25
3 Cammarata R C, Trimble T M, Srolovitz D J. Surface stress model for intrinsic stresses in thin films. J Mater Res, 2000, 15(11): 2468–2474
4 Chason E, Sheldon B W, Freund L B. Origin of compressive residual stress in polycrystalline thin films. Phys Rev Lett, 2002, 88(15): 156103
5 Hoffman R W. Stresses in thin-films-relevance of grain-boundaries and impurities. Thin Solid Films, 1976, 34(2): 185–190
6 Nix W D, Clemens B M. Crystallite coalescence: A mechanism for intrinsic tensile stresses in thin films. J Mater Res, 1999, 14(8): 3467–3473
7 Freund L B, Chason E. Model for stress generated upon contact of neighboring islands on the surface of a substrate. J Appl Phys, 2001, 89(9): 4866–4873
8 Sheldon B W, Ditkowski A, Beresford R, et al. Intrinsic compressive stress in polycrystalline films with negligible grain boundary diffusion. J Appl Phys, 2003, 94(2): 948–957
9 Chang C D, Yeh J J, Weng R J, et al. Simulation of nucleation and growth stages for sputtered films. Model Simul Mater Sci Eng, 2010, 18(2): 025010
10 Steven W L, Paulette C. A simple model for the growth of polycrystalline Si using the kinetic Monte Carlo simulation. Model Simul Mater Sci Eng, 2000, 8(5): 751–762
11 Hsueh C H. Modeling of elastic deformation of multilayers due to residual stresses and external bending. J Appl Phys, 2002, 91(12): 9652–9656
12 Hsueh C H. Thermal stresses in elastic multilayer systems. Thin Solid Films, 2002, 418(2): 182–188
13 Hsueh C H. Stress distribution and curvature in graded semiconductor layers. J Cryst Growth, 2003, 258(3-4): 302–309
14 Li J P, Fang M, He H B, et al. Model of stress evolution in polycrystalline oxide and composite thin films. Acta Opt Sin, 2012, 32(10): 301–305
15 Fang M, Hu D F, Shao J. Evolution of stress in evaporated silicon dioxide thin films. Chin Opt Lett, 2010, 8(1): 119–122
16 Shen Y, Shao S, He H, et al. Influences of thickness ratio of two materials on the residual stress of multilayers. Chin Opt Lett, 2007, 5(s1): 272–274
17 Zhang S, Zhang H, Zheng L, et al. Heat transfer in physical vapor deposition of polycrystalline multilayers and residual stress. In: ASME 2013 Heat Transfer Summer Conference. Minneapolis: American Society of Mechanical Engineers, 2013. V004T014A013
18 Ohring M. Materials Science of Thin Films. London: Academic Press, 2001
19 Read W T, Shockley W. Dislocation models of crystal grain boundaries. Phys Rev, 1950, 78(3): 275–289
20 Xiao N, Zheng C, Li D, et al. A simulation of dynamic recrystallization by coupling a cellular automaton method with a topology deformation technique. Comp Mater Sci, 2008, 41(3): 366–374
21 Shull A L, Spaepen F. Measurements of stress during vapor deposition of copper and silver thin films and multilayers. J Appl Phys, 1996, 80(11): 6243–6256
22 Incropera F P, De-Witt D P. Fundamentals of Heat and Mass Transfer. 2nd ed. New York: Wiley, 1985
23 Zhang S. Quick Practical Manual for New Metal Material Grades, Performance, Use and Foreign Brands. Hong Kong: China Science and Technology Culture Press, 2005
24 Haider J, Rahman M, Corcoran B, et al. Simulation of thermal stress in magnetron sputtered thin coating by finite element analysis. J Mater Proc Technol, 2005, 168(1): 36–41

Appendix A

The steady density of the island on the surface is obtained using the kinetic model of nucleation. In the model, the number of islands composed of different number of atoms changing with time can be expressed by

$$\begin{aligned}\frac{\mathrm{d}N_1}{\mathrm{d}t} &= \dot{R} - \frac{N_1}{\tau_\mathrm{s}} - K_1 N_1^2 - N_1 \sum_{i=2}^{\infty} K_i N_i, \\ \frac{\mathrm{d}N_i}{\mathrm{d}t} &= K_{i-1} N_1 N_{i-1} - K_i N_1 N_i,\end{aligned} \tag{a1}$$

where $\dot{R}$ is the rate that atoms come onto the surface and can be obtained by $p/\sqrt{2\pi mRT}$, where p is the pressure in the chamber and m is the molecular weight. τ_s is the remaining time of adatom on the surface and can be obtained as $v^{-1}\mathrm{e}^{E_\mathrm{a}/kT}$, where E_a is the adsorption energy. N_i is the numbers of islands of different numbers of atoms and K_i represents the rate constant. Using the partial equilibrium method, the steady density of islands on the surface is obtained as eq. (5). The parameters p' and E' in eq. (5) depend on the condensation regime of the deposition process and are summarized in Table a1.

In Table a1, the parameters i^* means the number of atoms that a critical nucleus contains. The number of atoms that a critical nucleus contains can be obtained by analyzing the thermal dynamic conditions for nucleation.

Table a1 Nucleation parameters p and E in eq. (5)

Regime	3D Islands	2D Islands
Extreme incomplete	$p'=(2/3)i^*$ $E'=(2/3)\left[E_{i^*}+(i^*+1)E_{\mathrm{des}}-E_{\mathrm{s}}\right]$	i^* $E_{i^*}+(i^*+1)E_{\mathrm{des}}-E_{\mathrm{des}}$
Initially incomplete	$p'=2i^*/5$ $E'=(2/5)\left(E_{i^*}+i^*E_{\mathrm{des}}\right)$	$i^*/2$ $(1/2)\left(E_{i^*}+i^*E_{\mathrm{des}}\right)$
Complete	$p'=i^*/(i^*+2.5)$ $E'=\left(E_{i^*}+i^*E_{\mathrm{s}}\right)/(i^*+2.5)$	$i^*/(i^*+2)$ $\left(E_{i^*}+i^*E_{\mathrm{s}}\right)/(i^*+2)$

During the deposition process, the free energy change of atoms can be expressed as:

$$\Delta\mu = kT\ln(p/p_0), \tag{a2}$$

where p_0 is the saturated vapor pressure under the given temperature.

The total energy change during nucleation process can be obtained as:

$$\Delta G = \Delta G_{\mathrm{V}} + \Delta G_{\mathrm{S}} = -\left(\frac{V}{V_0}\right)\Delta\mu + \sum S_i\gamma_i. \tag{a3}$$

The former part in eq. (a3) represents the free energy change during nucleation and the second part represents the surface energy change during nucleation. In eq. (a3), V is the volume of the nucleus which can be obtained by $4\pi r^3 f(\theta)/3$, where $f(\theta)=(2-3\cos\theta+\cos^3\theta)/4$ and θ is the contact angle which can be obtained from eq. (6). V_0 is the volume of a single atom, and S_i is the area of surfaces that formed when a nucleus is formed. The area of spherical cap can be expressed as $2\pi r^2(1-\cos\theta)$ and the area of the contact surface can be expressed as $\pi(r\sin\theta)^2$. γ_i is the surface energy of different surfaces that formed during the nucleation process. By solving $\mathrm{d}\Delta G/\mathrm{d}r=0$ the critical nuclear radius can be obtained as $r_c = 2V_0\gamma_{\mathrm{vl}}/\Delta\mu$. The number of atoms of a critical nucleus is then V/V_0. When the substrate has an angle of φ, the shape factor becomes $f(\theta,\varphi)=1-\sin(\theta+\varphi)/2-\cos^2(\theta+\varphi)\cos\theta/4\sin\varphi$.

The angle of substrate is formed when the islands coalesce and grow into columns. The angle can be expressed using the equilibrium relationship of surface energy and grain boundary energy.

$$\cos\frac{\varphi}{2} = \frac{1}{2}\frac{\gamma_{\mathrm{gb}}}{\gamma_{\mathrm{ls}}}. \tag{a4}$$

Appendix B

Suppose there are N' atoms in the metal and n' is on the surface, the total internal energy of the metal can be expressed as:

$$\begin{aligned} U_{\mathrm{A}} &= (N'-n')\frac{Z_0}{2}u_{\mathrm{AA}} + \frac{n'}{2}\left(Z_{\mathrm{s}}+\frac{Z_0-Z_{\mathrm{s}}}{2}\right)u_{\mathrm{AA}} \\ &= N'Z_0\frac{u_{\mathrm{AA}}}{2} - \frac{n'(Z_0-Z_{\mathrm{s}})}{4}u_{\mathrm{AA}}, \end{aligned} \tag{a5}$$

where u_{AA} is the potential energy between two atoms which is always a minus. The second term in eq. (a5) is the surface internal energy. Hence, the surface energy can be obtained for all metals:

$$\gamma = -\frac{n}{2}Z_\gamma u_{\mathrm{AA}}. \tag{a6}$$

The atom bonding energy can be obtained through heat of vaporization:

$$\Delta H_v = -\frac{N_0Z_0}{2}u_{\mathrm{AA}}. \tag{a7}$$

Combining eqs. (a6) and (a7), the surface energy can be obtained as eq. (7).

For the contact interface energy, if the two metals have a similar property, the interface energy will be about $\gamma_{\mathrm{AB}}=(\gamma_{\mathrm{A}}+\gamma_{\mathrm{B}})/4$; if the two metals have dissimilar property, the interface energy will be about $\gamma_{\mathrm{AB}}=(\gamma_{\mathrm{A}}+\gamma_{\mathrm{B}})/2$. γ_{A} and γ_{B} are the surface energies of each metal, separately.